Journal of Biomedical Optics

BiomedicalOptics.SPIEDigitalLibrary.org

Angularly resolved, finely sampled elastic scattering measurements of single cells: requirements for robust organelle size extractions

Ashley E. Cannaday
Janet E. Sorrells
Andrew J. Berger

SPIE.

Ashley E. Cannaday, Janet E. Sorrells, Andrew J. Berger, "Angularly resolved, finely sampled elastic scattering measurements of single cells: requirements for robust organelle size extractions," *J. Biomed. Opt.* **24**(8), 086502 (2019), doi: 10.1117/1.JBO.24.8.086502.

Angularly resolved, finely sampled elastic scattering measurements of single cells: requirements for robust organelle size extractions

Ashley E. Cannaday,[a,b] Janet E. Sorrells,[a,c] and Andrew J. Berger[a,*]
[a]University of Rochester, The Institute of Optics, Rochester, New York, United States
[b]Rollins College, Department of Physics, Winter Park, Florida, United States
[c]University of Illinois, Urbana-Champaign, Department of Bioengineering, Urbana, Illinois, United States

Abstract. Angularly resolved elastic light scattering is an established technique for probing the average size of organelles in biological tissue and cellular ensembles. Focusing of the incident light to illuminate no more than one cell at a time restricts the minimum forward-scattering angle θ_{min} that can be detected. Series of simulated single-cell angular-scattering patterns have been generated to explore how size estimates vary as a function of θ_{min}. At a setting of $\theta_{\text{min}} = 20$ deg, the size estimates hop unstably between multiple minima in the solution space as simulated noise (mimicking experimentally observed levels) is varied. As θ_{min} is reduced from 20 deg to 10 deg, the instability vanishes, and the variance of estimates near the correct answer also decreases. The simulations thus suggest that robust Mie theory fits to single-cell scattering at 785 nm excitation require measurements down to at least 15 deg. Notably, no such instability was observed at $\theta_{\text{min}} = 20$ deg for narrow bead distributions. Accurate sizing of traditional calibration beads is, therefore, insufficient proof that an angular-scattering system is capable of robust analysis of single cells. Experimental support for the simulation results is also presented using measurements on cells fixed with formaldehyde. [DOI: 10.1117/1.JBO.24.8.086502]

Keywords: angular scattering; elastic light scattering; single cell; Mie theory; microscopy.

Paper 190062RR received Mar. 12, 2019; accepted for publication Jul. 24, 2019; published online Aug. 24, 2019.

1 Introduction

Light scattering measurement techniques are useful for studying dynamic biological processes because they are nondestructive, noninvasive, and do not require exogenous labels. Angular elastic scattering, one such technique, can be used in order to obtain morphological information from biological samples, such as the mean size of cell organelles, which can yield important information about the health and behavior of the cells. Angular domain elastic scattering of cell suspensions and tissues has been used to diagnose precancerous conditions and observe subcellular changes in organelles during apoptosis.[1–4]

The angular scattering properties of the sample depend upon parameters such as size and refractive index. By comparing angular scattering patterns to a theoretical model, such scatterer characteristics can be determined. Mie theory[5] is a commonly used elastic scattering model for spherical scatterers with a diameter on the order of the incident wavelength. The scattered intensity depends on the scatterer size, refractive index of both the scatterer and the surrounding medium, the incident wavelength, the polarization of the incident light, and the scattering angle. For angular scattering, the results of Mie theory are particularly sensitive to small changes in scatterer size.[6] In the 1980s, generalized Lorenz-Mie theory (GLMT) was developed to describe elastic scattering using incident waves that are Gaussian rather than planar.[7–10] Scattering models other than Mie theory can be used to analyze angular scattering, including the T-matrix method[11] and complex focus theory.[12]

Angularly resolved forward scattering over broad ranges (from a few degrees to as high as 90 deg) with fine resolution (on the scale of 1 deg) has been modeled using Mie theory to estimate organelle size distributions in ensembles of cells. Mourant et al. calculated scatterer size distribution ranging from tens of nm to several microns in epithelial cells. Wilson et al.[13] used this approach to detect size distribution shifts associated with photodynamic therapy that targeted specific organelles (mitochondria and lysosomes, separately).[14,15] Both of these groups used scanning goniometers to obtain their angularly resolved data.

The motivation of the work described below is to extend this wide-angular-range, high-angular-resolution, Mie-based approach to the analysis of single cells. Forward-directed angular scattering is collected using an angular scattering microscope design inspired by Cottrell et al.,[16] rather than goniometric detection. Detecting a two-dimensional scattering pattern with fine angular resolution over a large angular range can be accomplished quickly, and it is a more light-efficient method of collecting the scattering from single cells.

Because we also aim to measure the scattering from a single cell that may have a neighbor, it is necessary to focus the excitation beam onto the sample plane. Angular scattering measurements of single cells over time would allow for the determination of differences in structure and behavior between individual cells. For the work presented in this paper, the excitation beam is focused to a subcellular spot size to ensure that only a single cell is illuminated. Due to the focusing of the beam to a sub-20 μm spot, a nontrivial portion of forward-scattering solid angle is obscured by unscattered light. This contrasts with studies that excite with a more collimated beam and correspondingly illuminate a larger region.

*Address all correspondence to Andrew J. Berger, E-mail: andrew.berger@rochester.edu

As such, a trade-off exits between the spot diameter and the measurable scattering angles. For example, a Gaussian spot size of 5-μm diameter (defined using the $1/e^2$ intensity width) using 785-nm light restricts angular measurements to 11 deg and higher. To have measurements down to 1 deg unobscured by unscattered light, the spot diameter has to increase to 55 μm. In addition to the limit imposed by the focused beam size, other practical effects further confine the range of analyzable scattering angles. If a physical mask is placed in the Fourier plane to prevent unscattered light from reaching the detector, flare around the edges of the mask, which can have sharp edges with some irregularities, can obscure additional angles.

Furthermore, measuring the scattering from single cells introduces several challenges. These include lower scattering intensities that must compete with the system background noise and speckle with larger grain size which can influence the fits to the data. Although the effect of the speckle grain can be reduced using a temporally incoherent excitation beam, broadband illumination washes out the Mie scattering features in the angular plane.[17]

In this paper, we present a study of the effect of angular range on the stability and accuracy of Mie theory fits to scattering from organelle-sized beads and from single cells. Simulated data permit investigation of behavior at the noise-free limit as well as at signal-to-noise levels typical of single-cell measurements on our current apparatus. Although several studies in the literature have extracted organelle size parameters of multiple-cell samples, to our knowledge no group to date has assigned uncertainties to size predictions derived from the angular scattering from a broad distribution of sizes similar to that of cell organelles. Here we also investigate the effect that angular range has on the uncertainty using computational methods. Experimental data from formalin-fixed single mammalian cells are also presented.

2 Methods

2.1 *Simulations*

Simulations were performed to test the effect of the detected angular range on the accuracy and precision of the fits to scattering from cell organelles. Scattering from an ensemble of spheres was simulated using GLMT using a linearly polarized excitation beam with a diameter of 7 μm and a simple addition of intensities. This method ignores any interference effects between spheres, which is a common approximation in the literature.[14,18–20] Three different size distributions were simulated: a narrow log-normal distribution of polystyrene beads with a mean diameter of 1 μm and a standard deviation of ± 0.015 μm, a single bead with a diameter of 5 μm, and a broad log-normal distribution of cell organelles with a mean diameter μ of 1.3 μm and a standard deviation σ of 0.6 μm. The first two distributions correspond to polystyrene beads that are used for routine calibration. The final distribution is a mitochondria-dominated distribution derived by Wilson et al.[15] from angular scattering analysis of squamous cell carcinoma suspensions. For this study, we assume a simplified model of the cell, in which the scattered light originates from a single population of scatterers (mitochondria, reported as the dominant light scatterers in the 10-deg to 60-deg forward-scattering range in some mammalian cell experiments[20]) so that the effect of minimum scattering angle alone could be isolated. (Comments about multiple population distributions are offered in Sec. 4.)

For each case, noise was added to the simulated scattering patterns that mimicked the observed noise in experimentally acquired scattering data. For the two bead cases, noise proportional to the square root of signal was used and scaled empirically to match the percentage seen in our experimental bead measurements (taken with a 50-ms exposure time and power of about 20 mW at the sample) to resemble shot noise. For single cell measurements, the small excitation beam diameter and multiple scatterers (organelles) in the sample result in speckle grains larger than single pixels of the detector array. Therefore, for the mitochondrial distribution, speckle noise was simulated by first adding white noise proportional to the signal square root, and then low-pass filtering the data. This resulted in scattering patterns with noise resembling speckle grain sizes and amplitudes observed in our single-cell experiments. Size distributions for each case and the resulting simulated scattering pattern with noise are shown in Fig. 1.

The simulated data were then modeled using Mie theory and a single-log-normal size distribution with mean size μ and width distribution σ. As described in Sec. 2.3, a least square error metric function given by Eq. (3) was minimized to identify the parameter pair (μ, σ) for the best theoretical fit. Predictions were performed 100 times with different simulated noises. The uncertainties in μ and in σ were defined as the standard deviation of the predictions from the 100 noise simulations. The standard error $\mathrm{SE}(x_i)$ of each uncertainty x_i was calculated by[21]

$$\mathrm{SE}(x_i) = \frac{x_i}{\sqrt{2N-2}}, \tag{1}$$

where $N = 100$.

To test the influence of angular range, size estimates were obtained as a function of the minimum detection angle $\theta_{\min}$, ranging from 5 to 20 deg. The maximum angle was held constant at 60 deg. Additional simulations were performed, in which $\theta_{\min}$ was fixed at 10 deg and the effect of decreasing the maximum angle was studied. Finally, in order to decouple the effects of angular range and speckle noise on the uncertainty in the size estimates, simulations were performed, in which the speckle grain size was also varied to more closely simulate the scattering from multiple cells at once. This allows us to compare the uncertainty in the estimates not only for various angular ranges, but also for single-cell and multicell scattering measurements.

2.2 *Experiments*

2.2.1 *Optical system*

Angular scattering data were acquired as described previously.[22] The angular scattering microscope diagram is shown in Fig. 2. Briefly, a collimated 785-nm diode laser source (I0785SU0050PA-TK, Innovative Photonic Solutions, Monmouth Junction, New Jersey) is linearly polarized and then directed through a condenser lens that produces a 14-μm spot size with a focusing half-angle of <5 deg and a power of ~20 mW at the sample.

Elastically scattered light is collected by a 1.3 NA oil-immersion microscope objective (N100×-PFO, Nikon Instruments, Tokyo, Japan). A 4f lens system images the back aperture of the objective onto a glass coverslip with an evaporated gold disc that rejects scattering angles of <8 deg, thus preventing unscattered light from reaching the detector. A second 4f system then

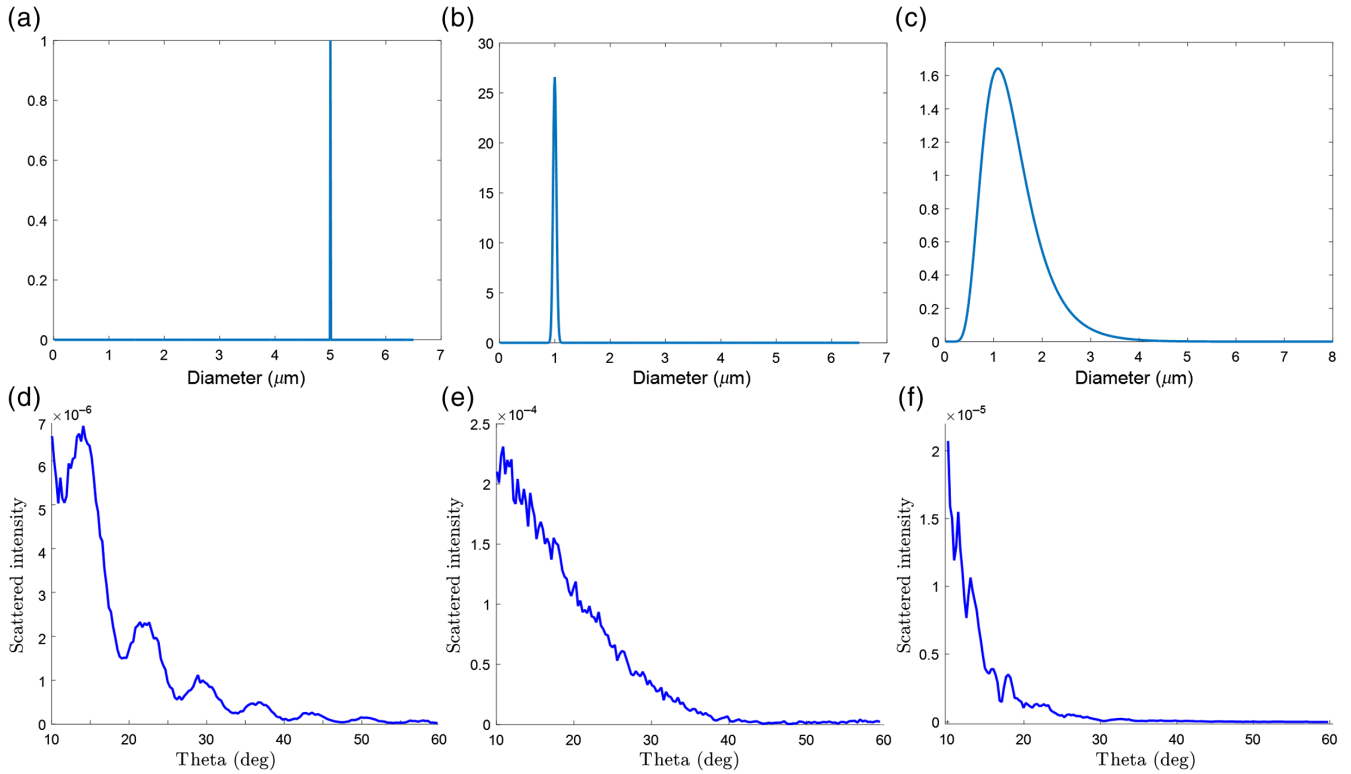

Fig. 1 (a)–(c) Simulated size distributions and (d)–(f) azimuthally averaged scattering patterns with noise for (a), (d) a 5-μm bead, (b), (e) a narrow distribution of 1-μm beads, and (c), (f) a broad distribution representing cellular mitochondria, all corresponding to a 50-ms exposure time. The speckle grains on the simulated mitochondria scattering span 6 to 7 pixels, while they are only 1 to 2 pixels wide in the bead scattering.

relays this Fourier image, referred to here as a scattergram, to a CCD array (640×480 pixels, 14-μm pixel pitch, Luca-S DL-658M-TIL, Andor Technology, Belfast, Northern Ireland). Images of the scattering pattern were acquired by summing five images with 10-ms exposure times.

2.2.2 *Bead sample preparation*

Bead samples were prepared for measurements by diluting one drop from the tip of the vial of polystyrene beads from a known size distribution in 10 mL of water. Approximately 0.5 mL of the bead dilution was placed on a coverslip in a sample chamber. The water was allowed to evaporate overnight, which adhered the beads to the glass coverslip due to electrostatic interactions. For measurements, the sample was rehydrated.

2.2.3 *Cell culture and preparation*

SCC7 mouse squamous cell carcinoma (ATCC, Manassas, Virginia, courtesy of the Foster Lab, University of Rochester Medical Center) were grown in an adherent monolayer in a Petri dish designed to promote cell adherence (Falcon standard tissue culture dishes, 08-772E, Fisher Scientific) and containing RPMI 1640 medium (Gibco, ThermoFisher Scientific) with 10% fetal bovine serum (Gibco) and antibacterial/antifungal agents (Plasmocin and Primocin, InvivoGen, San Diego, California). Cells were lifted from the dish using 0.25% trypsin (Gibco) and seeded into a new dish with round glass coverslips (12-546-1, Fisherbrand, Fisher Scientific, Pittsburgh, Pennsylvania) and media. The cells adhered to the coverslips, which were then removed from the dish and placed into an Attofluor cell chamber (A7816, Invitrogen, Carlsbad, California).

For fixation, the coverslip in the cell chamber was washed with phosphate-buffered saline (PBS) and the cells were then fixed by filling the chamber with 4% formaldehyde for 15 min at room temperature. The formaldehyde was aspirated and the cells were washed twice with PBS. The chamber was then filled with phenol red-free RPMI 1640 cell culture medium for cell measurements.

The chamber was placed in the sample plane of the system in a stage-top incubator (Stable "Z," Bioptechs, Butler, Pennsylvania) which provided heat from the objective lens and the perimeter of the chamber and allowed for the delivery of humidified 5% CO_2 to the cells. Although this study used only fixed cells, the temperature, humidity, and CO_2 settings were the same as for live cells in order to replicate all sources of uncontrolled variation. Prior comparisons between fixed and unfixed SCC7 indicated that the fixation process had little to no influence upon the measured scattergram. In this study, angular scattergrams were measured from one fixed cell repeatedly for 35 min.

2.3 *Data Fitting*

Each two-dimensional angular scattering pattern contained scattering signal as a function of polar angle θ (where $\theta = 0$ represents forward-directed unscattered light) and azimuthal angle ϕ. The data in each pattern were azimuthally averaged to produce a single vector $I(\theta)$ of scattered intensity versus polar

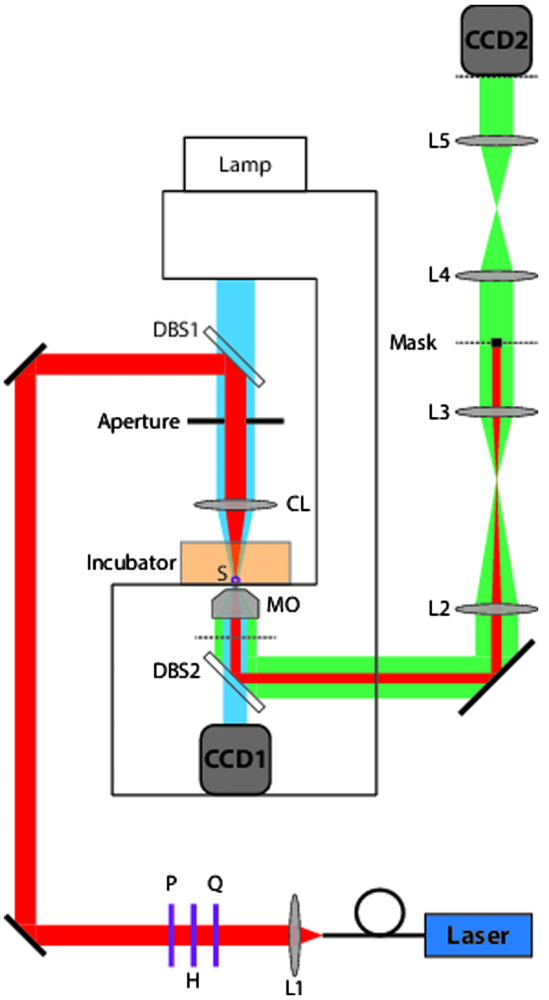

Fig. 2 Experimental setup for the angular elastic scattering system. Red, excitation beam; green, scattered light; blue, bright field illumination; L1 to L5, lenses; Q, quarter wave plate; H, half wave plate; P, polarizer; DBS1 and DBS2, dichroic beam splitters; CL, condenser lens; S, sample; MO, microscope objective; and mask, DC mask.

angle. The maximum analyzable angle (60 deg) is determined by the numerical aperture of our microscope objective. The minimum analyzable angle (θ_{min}) will be investigated here.

A theoretical model then determined the size distribution of Mie-scattering spheres that best explained the data. The same approach was used for fitting simulated and experimental $I(\theta)$ data. First, a lookup table of azimuthally averaged scattered intensity versus $\theta_{\text{min}} = 20$ deg and sphere diameter d was calculated using GLMT. θ ranged from 5 to 60 deg in steps of 0.275 deg, and d from 10 nm to 8 μm in steps of 10 nm. Then inspired by the work of Wilson et al.,[13] the ensemble of scatters was modeled as a single log-normal size distribution defined by a mean μ, a standard deviation σ, and an overall scaling parameter a (unitless, proportional to the total number of scatterers). Defining $I_{\text{theory}}(\theta)$ as the scattering dependence for $a = 1$, the best scaled fit $I_{\text{Stheory}}(\theta)$ for a given (μ, σ) pair was determined by linear least-squares optimization of

$$I_{\text{Stheory}}(\theta) = aI_{\text{theory}}(\theta) + b, \tag{2}$$

where b is a linear offset to compensate for experimental baseline drift.

The MATLAB downhill simplex function `fminsearch` was then used to estimate the best (μ, σ) pair by minimizing a χ^2-like error metric given by

$$M^2 = \sum_{\theta_{\text{min}}}^{\theta=60} [I_{\text{exp}}(\theta) - I_{\text{Stheory}}(\theta)]^2 + 10 \sum_{\theta=30}^{\theta=60} [I_{\text{exp}}(\theta) - I_{\text{Stheory}}(\theta)]^2. \tag{3}$$

Because angular scattering is much stronger at smaller values of θ, the second sum was included to boost the influence at the larger angles. The relative weight of 10 for this sum was selected empirically. Estimates were forbidden which resulted in the ratio of tail of the cross-section weighted size distribution to the peak being larger than a value of 0.1.

3 Results

3.1 *Simulation Results*

3.1.1 *Narrow bead distributions*

The uncertainty in the predicted mean diameter for the narrow simulated 1-μm bead distribution and the simulated single five micron bead was determined as a function of θ_{min} between 5 deg and 20 deg over 100 iterations of speckle noise. At the various angles, the uncertainty ranged from 4 to 17 nm for 1-μm bead fits, and 6 to 13 nm for 5-μm scattering, in neither case with any pattern versus angle. These uncertainties are on the order of our Mie theory lookup table diameter step size of 10 nm.

Figure 3 shows representative maps of $1/M^2$ [the inverse of the error metric in Eq. (3)] as a function of the two log-normal size population parameters μ and σ. $1/M^2$ is normalized in each plot to a maximum of 1, which corresponds to the best fit (smallest value of M^2.) Maps are shown for the two simulated bead diameters and for θ_{min} values of both 20 deg and 10 deg. Because of physical assertions about the size distributions (e.g., requiring the distribution weight to be close to zero at $d = 0$), a zone of forbidden predictions exists near the bottom of the plots (shown in dark blue).

The error maps have step sizes of 100 nm in the μ dimension; on this scale, the best fit is confined to a single pixel. As noted above, the fluctuation in the selected μ value over the 100 simulations is on the scale of 10 nm. The error maps also indicate that in three of the four cases, the fit correctly estimates the population width σ to be as close to zero as possible. The only exception occurs at $\theta_{\text{min}} = 20$ deg, where the best fit for the 1 μm beads is $\sigma \approx 75$ nm. Switching to $\theta_{\text{min}} = 10$ deg eliminates this error. Overall, the error metric maps for the two different minimum angles are similar for both the large and small bead diameter cases. This further supports the argument that θ_{min} does not have a significant impact on the uncertainty of the fits to narrow bead distributions.

3.1.2 *Mitochondria distribution*

When the population width is broader, angular scattering becomes less sensitive to changes in μ. Although the effect is clear when the narrow-width pattern has multiple peaks, e.g., see Figure 11.6 in Ref. 6), it is less obvious for monotonically decreasing scattering. To illustrate the effect, Mie theory plots for a 1-μm bead and for the mitochondria-like size distribution

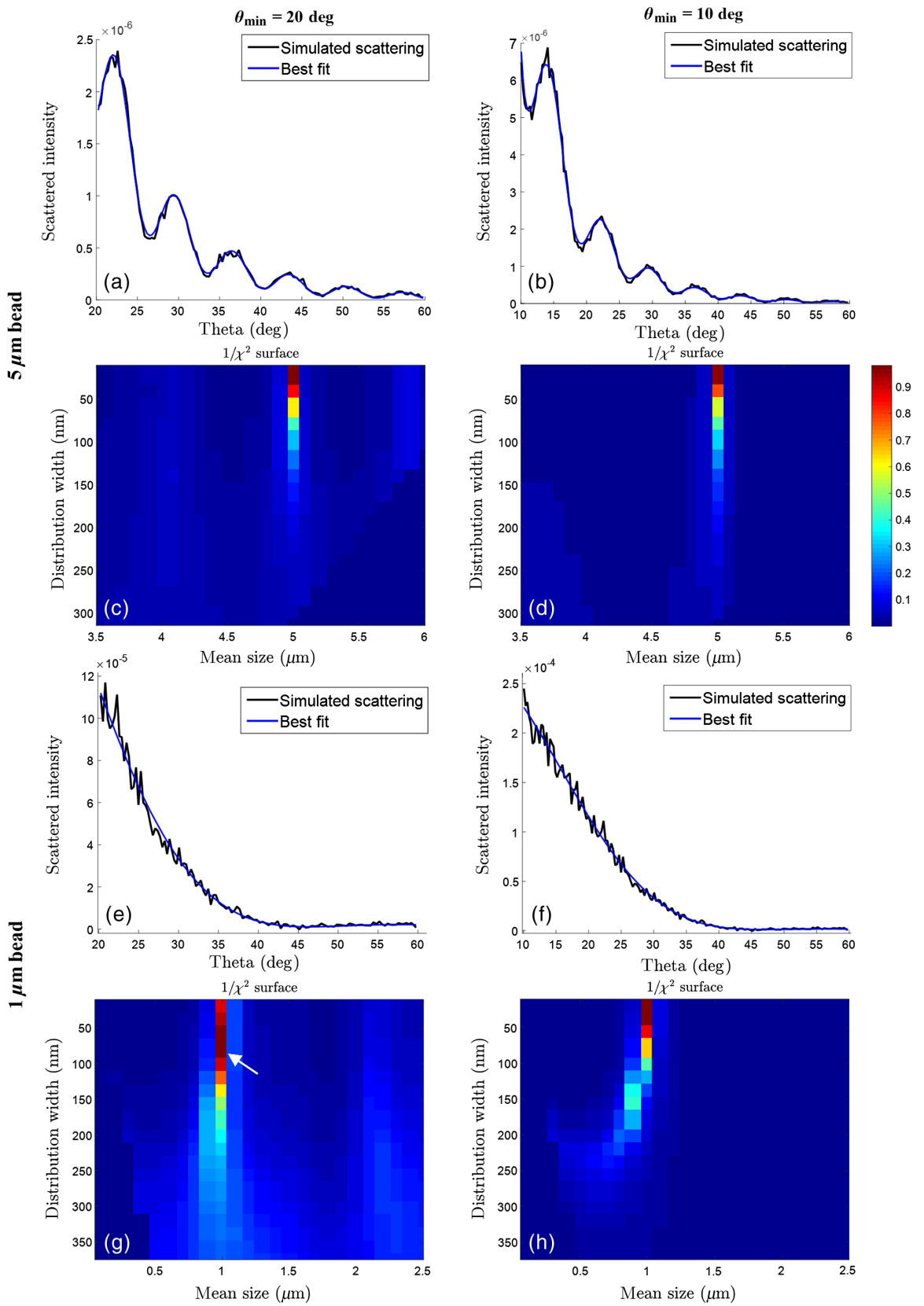

Fig. 3 Best theory fits to an example simulated 5-μm scattering using (a) $\theta_{\text{min}} = 20$ deg and (b) $\theta_{\text{min}} = 10$ deg. Normalized error metric maps for this example are also shown for (c) $\theta_{\text{min}} = 20$ deg and (d) $\theta_{\text{min}} = 10$ deg. Fits resulting in the lowest error (i.e., best fits) are shown in the red areas of the maps. Also shown is an example of the simulated scattering for a 1-μm bead and the best theory fits using (e) $\theta_{\text{min}} = 20$ deg and (f) $\theta_{\text{min}} = 10$ deg; (g), (h) the error metric maps for each θ_{min}. The arrowhead indicates the one global best fit that incorrectly selected a nonzero σ parameter.

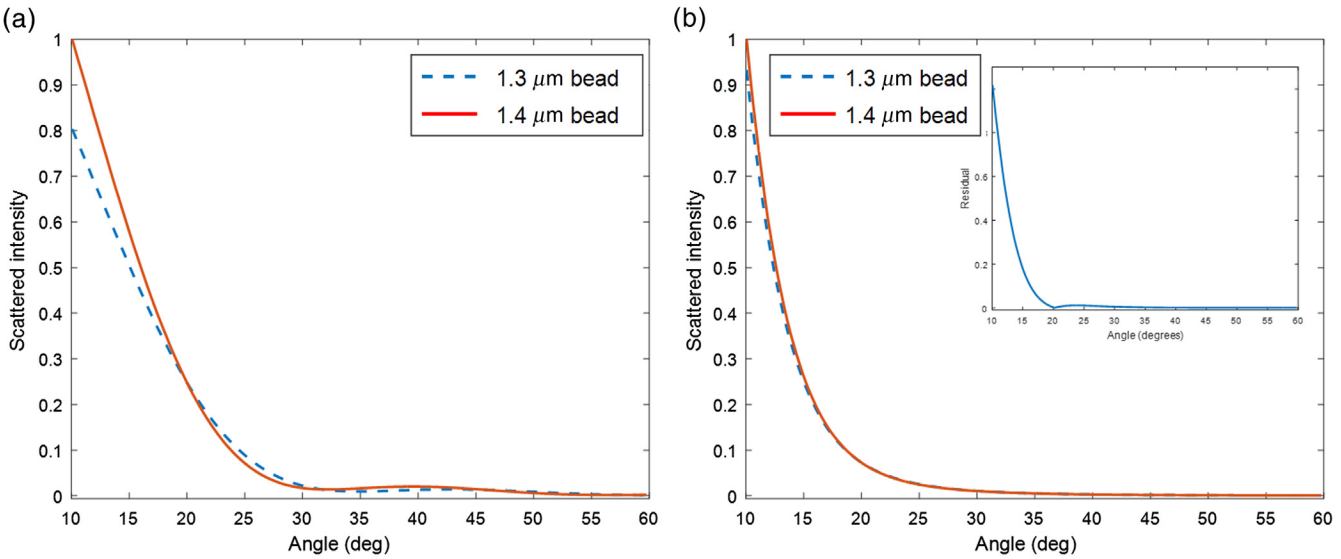

Fig. 4 Theoretical scattering curves (a) for 1.3- and 1.4-μm-diameter beads and (b) for broad distributions ($\sigma = 0.6$ μm) with μ values of 1.3 and 1.4 μm. A 100-nm change in μ results in visibly distinguishable scattering curves for the narrow bead distribution. The same change in μ for the broad distribution produces less change overall, and the residual (inset) shows the change to be concentrated at angles less below 20 deg.

($\mu = 1.3$ μm and $\sigma = 0.6$ μm) are shown in Fig. 4. In each plot, the scattering for a 100-nm increase in μ is also shown, with the two curves scaled to match at $\theta = 20$ deg. For the 1-μm bead, a 100-nm change in diameter causes a visible change in the angular dependence both above and below 20 deg, which explains why the parameter maps in Fig. 3 have sharp maxima regardless of θ_{min}. For the mitochondrial distribution, however, the scattering changes are much smaller. The inset, showing the absolute value of the residual, shows that changes are now more concentrated at angles below 20 deg. This suggests that, unlike with narrow bead distributions, using $\theta_{\text{min}} = 10$ deg instead of 20 deg should confer greater sensitivity to μ.

When maps similar to those in Fig. 3 are generated for the simulated mitochondrial population ($\mu = 1.3$ μm and $\sigma = 0.6$ μm) show that θ_{min} has a significant effect on the stability of the size predictions. Example error metric maps for simulated single cell scattering are shown in Fig. 5. In both cases the value of $1/M^2$ has a local maximum near $\mu = 1.44$ μm and $\sigma = 600$ nm. For $\theta_{\text{min}} = 20$ deg, there are also local maxima for μ near 3 and 5 μm with comparable $1/M^2$ values. When the simulated noise was varied 100 times, the global best fit lay in these incorrect lobes of solution space 40% of the time. The extra lobes are absent for $\theta_{\text{min}} = 10$ deg, as shown in this figure, and the primary lobe shrinks. We found that values of θ_{min} of <15 deg were sufficient to prevent global maxima occurring outside of the primary lobe.

To emphasize the greater robustness at lower angles, Fig. 5(c) (bottom) shows two $\theta_{\text{min}} = 20$ deg fits corresponding to the local maxima in (μ, σ) space marked by asterisks in panel a. Both fits follow the data to within the noise. When those two fits are extended to $\theta_{\text{min}} = 10$ deg in panel d, the fit from the incorrect lobe (asterisk 2) deviates drastically from the simulated data at the added angles.

Even if solutions from the other lobes are rejected (e.g., by restricting the range of accepted values), Fig. 5's error maps also reveal that $1/M^2$ is more sharply peaked around its maximum for $\theta_{\text{min}} = 10$ deg. The dashed line in (a) traces the contour of fits with $1/M^2 = 0.7$, i.e., a moderately good fit relative to the maximum of 1.0. This same contour line is overlaid on the $\theta_{\text{min}} = 10$ deg error map, showing that the new area of fits with $1/M^2 \geq 0.7$ is now smaller.

For these simulated cell distributions, the uncertainty of the predicted μ and σ as a function of θ_{min} was determined by calculating the standard deviation of the predictions as the speckle noise was simulated 100 times, and is plotted in Fig. 6. The uncertainty in the predicted mean drops as θ_{min} is decreased, until it plateaus around 14 deg. The uncertainty in the predicted population width σ continues to decrease as θ_{min} is decreased lower than 14 deg (data not shown). These results illustrate the importance of collecting angles below 20 deg when performing fits, in which μ and σ are both free parameters. At the other end of the angular range, varying θ_{max} from 30 deg to 65 deg produced no significant change in the uncertainty of the predictions for $\theta_{\text{max}} > 35$ deg.

Note that the error maps shown in Fig. 5 are idiosyncratic to the particular speckle noise generated for one simulation. At $\theta_{\text{min}} = 10$ deg, according to the upper uncertainty plot of Fig. 6, another noise iteration would produce a map where the best fit has a μ value up to ± 200 nm different from the previous one. For the $\theta_{\text{min}} = 10$ deg error map of Fig. 5, points that are ± 200 nm horizontally displaced from the best fit (asterisk 1) have $1/M^2$ values close to 0.7. This suggests a new way to read the error map: that all points with $1/M^2$ values of 0.7 are (μ, σ) pairs that could be optimal for another instance of speckle noise on the same underlying Mie pattern. We will return to this line of reasoning when discussing experimental measurements of a fixed cell.

These simulations were repeated using a smaller speckle grain, as would occur if there were contributions over a larger field of view from multiple cells. The results were qualitatively the same: secondary lobes appeared in the $1/M^2$ map for $\theta_{\text{min}} = 20$ deg, and this phenomenon ceases to exist at $\theta_{\text{min}} = 10$ deg. Additionally, as shown in Fig. 6, the uncertainty in μ significantly improved versus reduction in θ_{min} until around 15 deg.

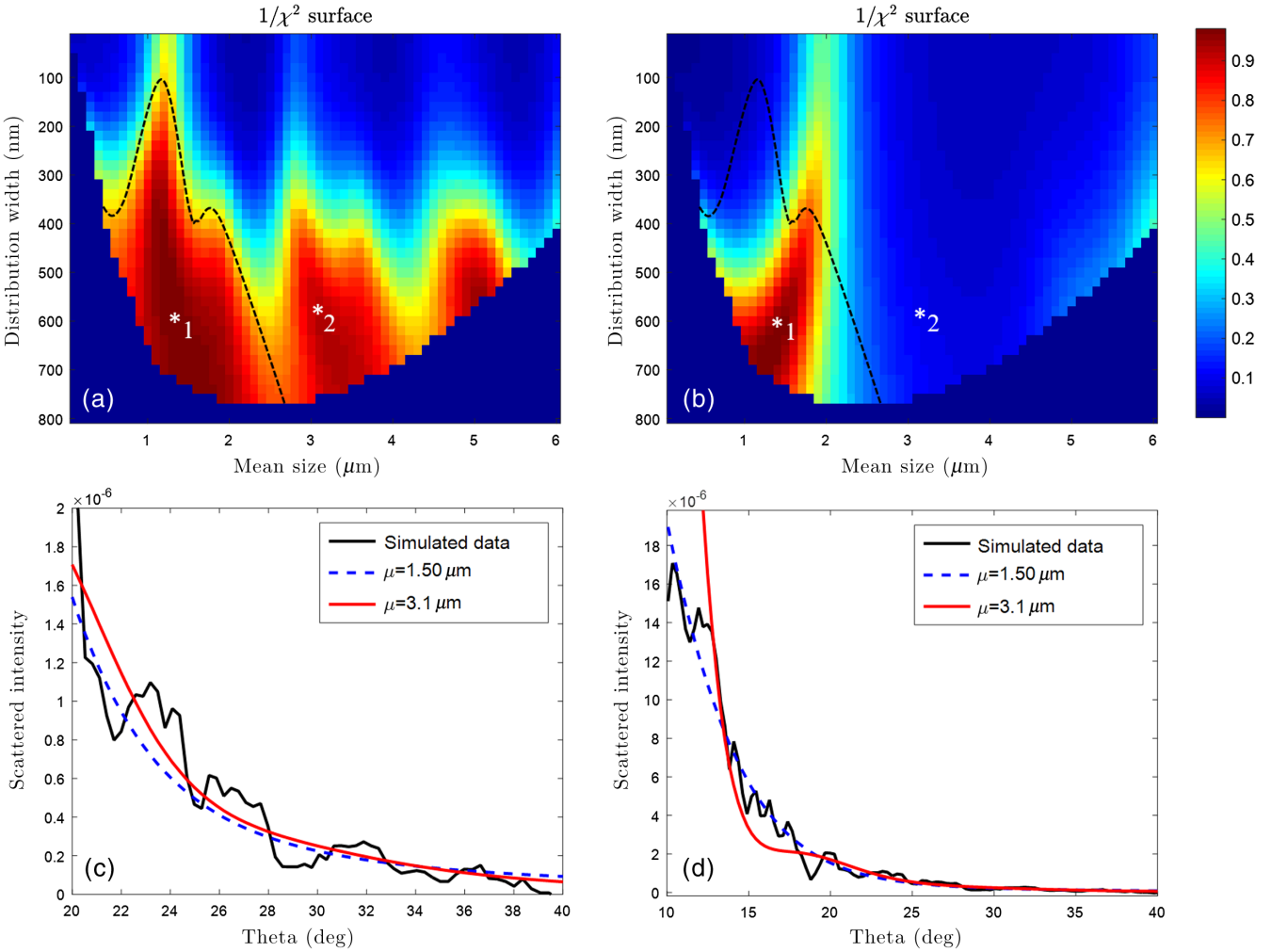

Fig. 5 (a), (b) Example error metric maps for fits to cell scattering using θ_{min} of (a) 20 deg and (b) 10 deg. The contour line for $1/M^2 = 0.7$ in (a) is marked with a dashed line and is also overlaid on (b). (c) Comparison of fits to simulated data using (μ, σ) parameters at the two points marked by asterisks in (a). The two fits produce similar $1/M^2$ values. (d) Same fits extended to $\theta_{min} = 10$ deg, showing that the fit from asterisk 2 in the incorrect lobe deviates drastically from the data at lower angles.

Unsurprisingly, the absolute uncertainty at low angles is lower for the smaller speckle grain size. From these results, we can conclude that measuring lower scattering angles is crucial not only for single-cell measurements, but also for multicell measurements.

3.2 *Experimental Results*

3.2.1 *Polystyrene bead measurements*

As expected from our simulations of beads, theory fits to experimental scattering measurements from single beads did not result in striking differences in the predicted diameter as a function of θ_{min}. Representative plots for one 5-μm and one 1-μm diameter bead are shown in Fig. 7. Plausible size predictions are obtained when the beads' azimuthally averaged scattering patterns are fit over the angular range of 20 deg to 60 deg [Fig. 7(a)]. Figure 7(b) shows similar fits and size predictions when fits are performed using $\theta_{min} = 10$ deg.

Estimates of σ for 20 single-5-μm beads are summarized by box plots in Fig. 8. Angular scattering from 20 different single-5-μm beads was fit using θ_{min} values of 10 deg and 20 deg. The average predicted μ did not differ significantly when θ_{min} was reduced from 20 deg to 10 deg. However, the σ of the distribution was predicted more accurately using $\theta_{min} = 10$ deg. Because only a single bead at a time was measured, the predicted σ for each fit should be close to zero. Because our fitting algorithm cannot choose a width of zero, the minimum possible width prediction was the 10-nm step size of the theory lookup table. A Wilcoxon rank-sum test showed the distribution of σ values for the $\theta_{min} = 20$ deg analysis to be significantly different ($p < 0.001$), and according to Fig. 8 clearly larger, which is less accurate.

It is worth noting that the single 1-μm beads were sized accurately only if the width of the size distribution was forced to be zero. When the width was a free parameter, regardless of θ_{min}, the fits resulted in predicted means that were smaller than the manufacturer specifications (typically about 0.8 to 0.9 μm) and large distribution widths (100 to 200 nm). This is most likely because of lower signal-to-noise due to the reduced scattering signal from the smaller diameter bead.

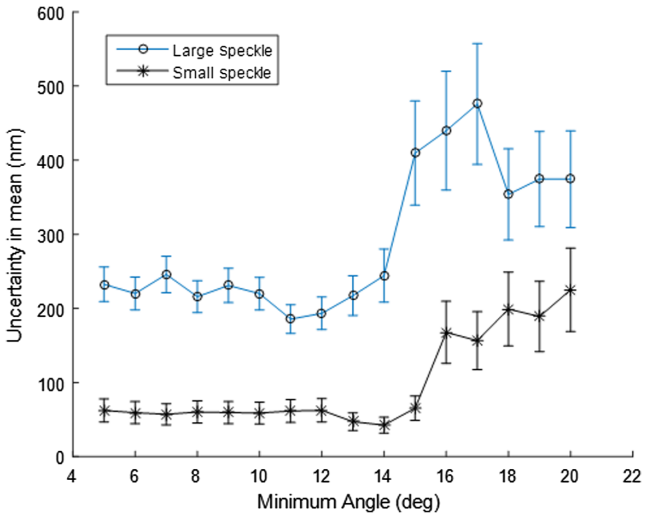

Fig. 6 Uncertainty in the prediction of μ as a function of $\theta_{\min}$ for two speckle grain sizes corresponding to single-cell and multicell measurements. Estimates from secondary minima have been excluded from the calculations. Bars are plotted depicting the standard error in the uncertainty, as given in Eq. (1). For both levels of speckle, the uncertainty decreases as $\theta_{\min}$ is lowered below 20 deg at first, and then plateaus.

3.2.2 *Single-cell measurements*

The experimental scattering pattern, azimuthal average, and resulting best Mie theory fit from a single fixed cell are shown in Fig. 9. The theory curve is fit to the data to within the noise, whose amplitude is dictated by the large speckle grains. Figure 10 shows the corresponding error metric map for a typical cell as a function of size distribution mean and width for $\theta_{\min} = 20$ deg and 10 deg, similar to those shown in the simulation results.

From the experimental error maps, we see that the best fits cluster at population widths σ that are noticeably larger than 0. This effect is more pronounced for $\theta_{\min} = 10$ deg. No single-scatterer size is able to model the intensity falloff of the single-cell data over the entire angular fitting range. Our single-cell scattering data are only well to within the noise when a broad distribution of sizes is modeled, as one would expect *a priori*.

The experimental single-cell $1/M^2$ map for $\theta_{\min} = 20$ deg (Fig. 10, left) exhibits multiple local maxima in the $1/M^2$ map. This is evocative of the results of the simulated organelle scattering (cf., Fig. 5). The $\theta_{\min} = 10$ deg map has only one local maximum lobe, again in parallel with simulations. Recall from the simulations that the true (μ, σ) value for a single-log-normal population could be assigned a $1/M^2$ value as low as 0.7 due to speckle noise. The region of $1/M^2$ values greater than 0.7 for the experimental $\theta_{\min} = 10$ deg results (outlined in the plot) contains estimates with μ values in the range 0.8 to 0.9 μm; two such points in that regime are indicated by asterisks.

In addition, the $\theta_{\min} = 10$ deg estimates of μ for the fixed SCC7 cell fluctuated less over 35 min even when the $\theta_{\min} = 20$ deg solution space was confined near the correct lobe. Using $\theta_{\min} = 20$ deg, the estimated μ drifted slowly between 300 and 600 nm over the 35 min. When analysis included angles down to 10 deg, estimates stayed steady to within 30 nm.

4 Discussion

4.1 *Beads*

Measurements of single beads or bead ensembles with known size distributions are commonly used to calibrate an angular scattering system and ensure that good quality data and fits are being obtained.[16,17,22,23] For single beads or narrow size distributions of scatterers, analyzing the scattering down to only 20 deg is sufficient for estimating mean diameter. In our simulations, changing to $\theta_{\min} = 10$ deg did not significantly change the uncertainty in the predicted sizes for either large (5 μm) or small (1 μm) diameter beads (cf., Fig. 3). This matches our experimental experience with bead measurements (cf., Fig. 7).

Even for single beads, however, there was a benefit to incorporating lower angles. Fits to single-5-μm bead scattering using $\theta_{\min} = 10$ deg consistently returned σ estimates near zero as was correct, while analysis using $\theta_{\min} = 20$ deg did not (cf., Fig. 8).

4.2 *Cells*

The results above for beads invite the thought that $\theta_{\min} = 20$ deg might produce similarly acceptable results for cell organelle analysis. As noted by Bohren and Huffman,[6] however, the heterogeneity in broader distributions blurs the features in the scattering patterns. When we fit the simulated scattering from cell organelle-like size distributions, results for $\theta_{\min} = 20$ deg were markedly inferior in two ways to those obtained at $\theta_{\min} = 10$ deg. First, there were multiple local maxima in (μ, σ) solution space for $\theta_{\min} = 20$ deg, and realistic levels of measurement noise were sufficient to vary which location was the global maximum; this effect vanished for $\theta_{\min} = 10$ deg. Second, in the neighborhood of the true (μ, σ) values, the $1/M^2$ map was less sharply peaked for $\theta_{\min} = 20$ deg than for $\theta_{\min} = 10$ deg. For our empirically observed level of speckle noise, there appears to be a crucial turning point in the cell scattering curve at ~15 deg, as is shown in Fig. 6. As a result, the fits to these lower angles are not simply more accurate because more scattering angles are included, but because there is a shape change in the scattering versus angle curve specifically at the low angles that must be included to obtain accurate and stable fits.

This behavior was not seen in the size predictions from narrower size distributions, as the effect ultimately arises from the broad distribution of organelle sizes in the cell. Experimental measurement specifications that are sufficient for sizing narrow bead distributions may be insufficient for analyzing broader distributions. This highlights that validating an angular scattering system using narrow bead distributions, a common step in the angular scattering literature, is necessary but not sufficient to ensure that the system will work for cells, i.e., for broad distributions of organelle sizes. The results indicate that speckle grain size influences the prediction accuracy. Single cells have a maximum distance between scatterers dictated by the size of the cell, leading to larger speckle grains than if multiple cells contribute to the measurement. In turn, the simulation results in Fig. 6 show that the larger speckle grains associated with single cells lead to a larger uncertainty in estimates of μ, even when the lowest angles are incorporated. For single cells, the simulation reported an uncertainty of ~200 μm; for a grain size approximately five times smaller, it dropped to 50 μm. The likely reason is that a larger speckle grain pulls a larger amount of the lowest-angle

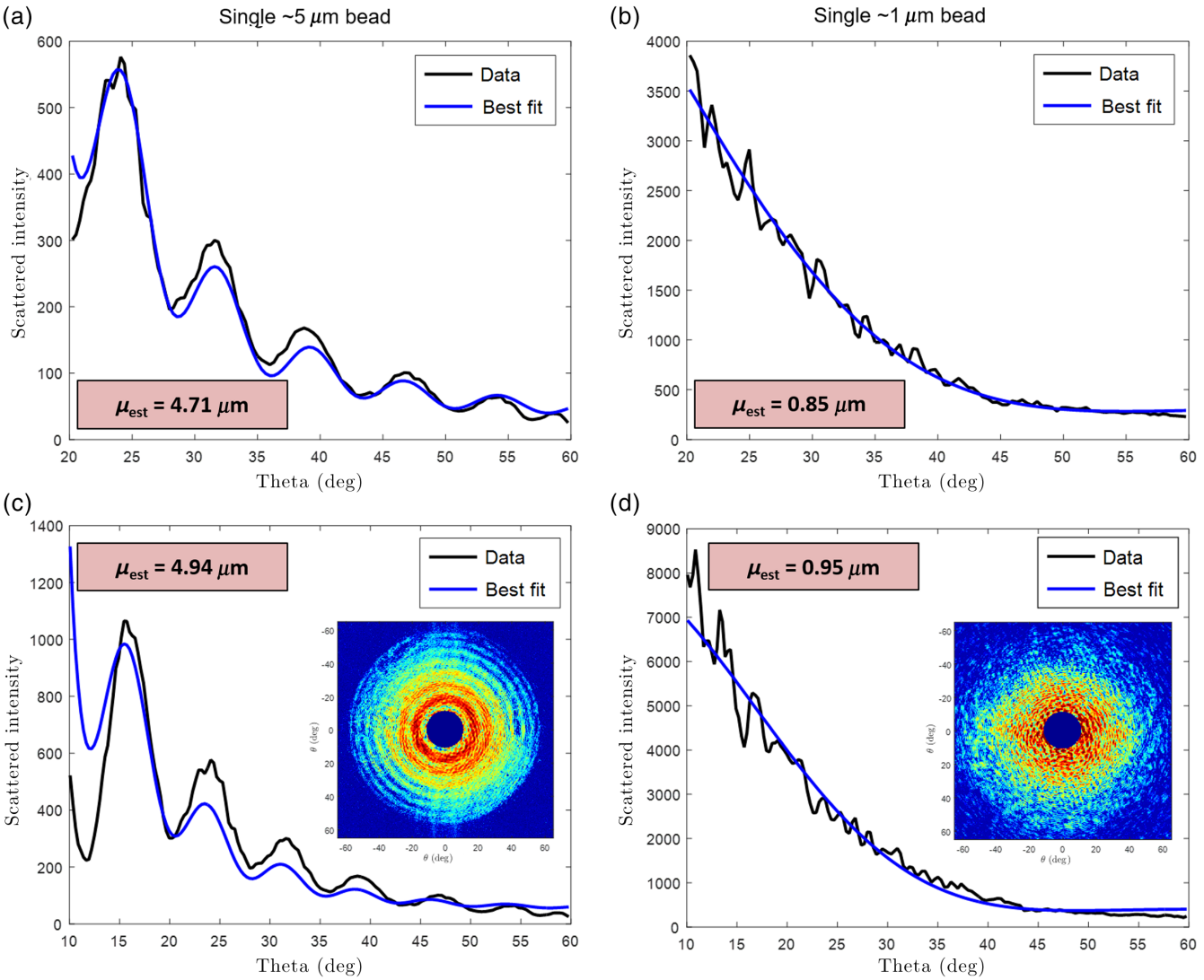

Fig. 7 (a), (b) Best Mie fits to experimental azimuthally averaged angular scattering over the 20-deg to 60-deg angular range for (a), (c) a single-5-μm bead; (b), (d) a 1-μm bead. (c), (d) Fits to the same data using $\theta_{\text{min}} = 10$ deg. Size estimates from the best fit to Mie theory are given for each case. Insets show the two-dimensional scattergrams.

data in the same direction, and perturbations at the lowest analyzed angles affect the fit parameters most radically.

Even when $\theta_{\text{min}} = 10$ deg is used, the single-cell angular scattering data given here can be modeled by Mie theory to within the noise using a single-log-normal size distribution. Previous work by Mourant et al.[13] and Wilson and Foster[20] using goniometers has modeled angular scattering from cell suspensions to two or more populations of scatterers, and Wilson et al. specifically illustrated that a single population was inadequate to fit their angular data. There are at least two differences in the cell measurements performed here. First, our microscope-based instrument measured down to 10 deg, as compared to 3 deg in Ref. 18. Had our single cells been measured down to 3 deg, a single-population fit might not have been adequate. Second, the speckle grains in a single cell measurement distort the data more. They are larger both in angular extent (due to the reduced area over which the scattering is emitted, as discussed above) and in amplitude (because there is no averaging from multiple cells or from cell motion in suspension). Efforts are underway in our group to mitigate both the angular limitations and the speckle effects.

Compared to the simulation results in Fig. 5(b), the region of best fits ($1/M^2 > 0.7$) in the SCC7 cell's $\theta_{\text{min}} = 10$ deg error map [Fig. 10(b)] was pushed to lower μ and σ values overall. The direction of this shift is unsurprising, given that the simulation contained solely a mitochondrially inspired population distribution with a mean of 1.3 μm (from Ref. 15), while the experimental measurement of an intact cell included smaller organelles. The best-fit region contained μ values as high as 0.9 μm, which is a plausible intermediate value between mitochondria and smaller organelles, given that the current fits are limited to a single population as discussed in the previous paragraph. In addition to reducing the speckle amplitude and the minimum measured scattering angle, more work is needed to establish both (a) a range of (μ, σ) estimates obtained for single SCC7 cells by angular scattering and (b) reference information about the actual organelle size distribution within such cells.

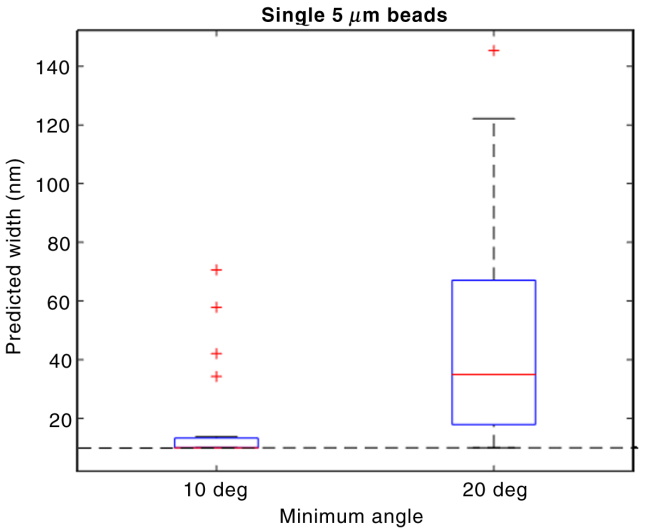

Fig. 8 Boxplots of the predicted σ for 20 single-5-μm bead measurements using a θ_{min} of either 10 deg and 20 deg. A dashed line indicates the 10-nm step size of the lookup table, which corresponds to the correct width prediction for a single-bead measurement. The plots indicate that fits to the data using a minimum angle of 10 deg result in more consistently narrow width predictions.

This study showed that the size estimates for a fixed cell were dramatically more stable over 35 min when angles below 20 deg were included in the analysis. For $\theta_{min} = 10$ deg, the stability was at the 30-nm level. This does not mean that the estimates were accurate. We believe that when angular scattering is performed on single adherent cells using $\theta_{min} = 10$ deg, the limit on the accuracy is imposed by the speckle. In this case, because the cell was fixed, the speckle remained largely the same throughout the 35 min, hence the best Mie fit kept nearly the same parameters. For the $\theta_{min} = 20$ deg case, the measurement-to-measurement variations due to shot noise and system drift were enough to make the Mie fits unstable. With the added angular information between 10 deg and 20 deg, the data analysis stabilized, but we emphasize that reducing the speckle in single-cell measurements is the essential next step for replicating the accuracy of multicell organelle sizing analysis in single cells using angular scattering.

As previously mentioned, the aim of this work is to extend wide-range/high-resolution angular scattering plus Mie analysis to the single-cell regime to obtain scatterer size distributions. There are other methods of deriving size distributions in single cells from variations in angular scattering. Zhang and Boustany[24] used optical scatter image ratio (OSIR) to assign scatterer sizes to subdomains of a cell image and thus obtain scatterer size distribution estimates for the cell as a whole. In that work, two wide-field images of cells were acquired at different numerical apertures. A two-element vector of angular information is thus built up at each pixel, sufficient for Mie theory to estimate a sphere diameter at each location, from which the size distribution emerges. Scatterer motion and objects larger than the pixel size introduce error into the estimation process. Here, by comparison, a large number (>100) of angular values is obtained from the illuminated area. A benefit is that this enables multiparameter fitting to the angular data, extracting not just a sphere size but other moments of the size distribution. On the other hand, the multiparameter fit must assume a functional form (here, a log-normal distribution) whose validity will vary by case, especially for cells with smaller numbers of significant scatterers. Another downside is that all spatial information within the cell is lost by the nature of the Fourier-domain intensity measurement. We note that angular scattering from single transilluminated cells can also be obtained by Fourier-transform of a complex-field image.[25–27] To our knowledge, however, inversions of such angular data by Mie theory to obtain size distributions of nonnuclear organelle populations have not been reported.

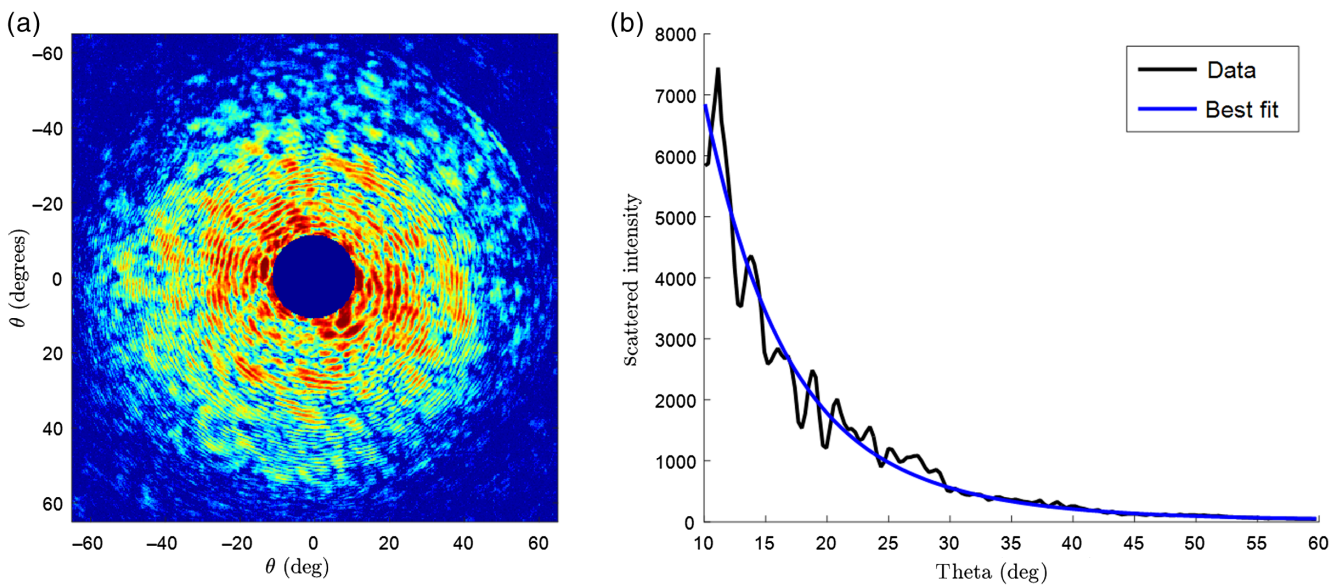

Fig. 9 (a) Experimental angular scattergram and (b) azimuthal average of scattered intensity versus angle with best fit for a typical single fixed cell measurement. The fit parameters were $\mu = 0.32$ μm and $\sigma = 230$ nm.

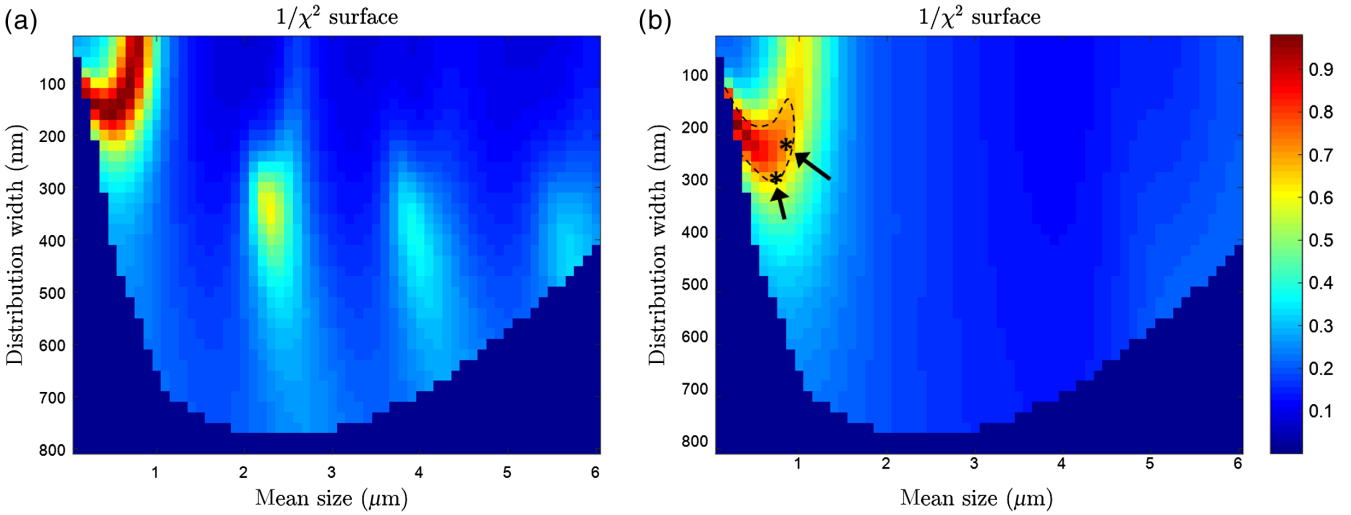

Fig. 10 Normalized $1/M^2$ maps for a log-normal distribution fit to the data of Fig. 9 using (a) $\theta_{min} = 20$ deg and (b) $\theta_{min} = 10$ deg. The top row of each plot represents the error with a width of zero, i.e., a fit with a single particle size. Note the secondary maxima exhibited in the $\theta_{min} = 20$ deg plot, analogous to the simulated cell data in Fig. 5. In the $\theta_{min} = 10$ deg plot, the dashed contour line encloses the $1/M^2 > 0.7$ region of statistically equivalent fits, as in Fig. 5. Asterisks indicate two representative points within that region (μ, σ) values of (0.8 μm and 280 nm) and (0.9 μm and 220 nm) with means that are intermediate between expected values for mitochondria and smaller organelles.

Disclosures

The authors have no relevant financial interests in this article and no potential conflicts of interest to disclose.

Acknowledgments

The authors thank Tim Baran and Thomas Foster for helpful conversations and support with cell culturing. This work was partially supported by NSF CBET award No. 1402345 (Biophotonics).

References

1. L. T. Perelman et al., "Observation of periodic fine structure in reflectance from biological tissue: a new technique for measuring nuclear size distribution," *Phys. Rev. Lett.* **80**(3), 627–630 (1998).
2. V. Backman et al., "Polarized light scattering spectroscopy for quantitative measurement of epithelial cellular structures in situ," *IEEE J. Sel. Top. Quantum Electron.* **5**(4), 1019–1026 (1999).
3. Y. L. Kim et al., "Simultaneous measurement of angular and spectral properties of light scattering for characterization of tissue microarchitecture and its alteration in early precancer," *J. Sel. Top. Quantum Electron.* **9**(2), 243–256 (2003).
4. N. N. Boustany et al., "BCL-xL-dependent light scattering by apoptotic cells," *Biophys. J.* **87**(6), 4163–4171 (2004).
5. G. Mie, "Beiträge zur optik trüber medien, speziell kolloidaler metallösungen," *Annalen der Physik* **330**(3), 377–445 (1908).
6. C. F. Bohren and D. R. Huffman, *Absorption and Scattering by Small Particles*, Wiley Interscience, New York (1983).
7. G. Gouesbet, G. Grehan, and B. Maheu, "Scattering of a Gaussian beam by a Mie scatter center using a Bromwich formalism," *J. Opt.* **16**(2), 83–93 (1985).
8. G. Gouesbet, B. Maheu, and G. Grehan, "The order of approximation in a theory of the scattering of a Gaussian beam by a Mie scatter center," *J. Opt.* **16**(5), 239–247 (1985).
9. G. Grehan, B. Maheu, and G. Gouesbet, "Scattering of laser beams by Mie scatter centers: numerical results using a localized approximation," *Appl. Opt.* **25**(19), 3539–3548 (1986).
10. G. Gouesbet, G. Grehan, and B. Maheu, "Localized interpretation to compute all the coefficients GMN in the generalized Lorenz-Mie theory," *J. Opt. Soc. Am. A* **7**(6), 998–1007 (1990).
11. M. G. Giacomelli et al., "Application of the T-matrix method to determine the structure of spheroidal cell nuclei with angle-resolved light scattering," *Opt. Lett.* **33**(21), 2452–2454 (2008).
12. N. J. Moore and M. A. Alonso, "Closed form formula for Mie scattering of nonparaxial analogues of Gaussian beams," *Opt. Express* **16**(8), 5926–5933 (2008).
13. J. R. Mourant et al., "Polarized angular dependent spectroscopy of epithelial cells and epithelial cell nuclei to determine the size scale of scattering structures," *J. Biomed. Opt.* **7**(3), 378–387 (2002).
14. J. D. Wilson et al., "Light scattering from intact cells reports oxidative-stress-induced mitochondrial swelling," *Biophys. J.* **88**, 2929–2938 (2005).
15. J. D. Wilson, W. J. Cottrell, and T. H. Foster, "Index-of-refraction-dependent subcellular light scattering observed with organelle-specific dyes," *J. Biomed. Opt.* **12**(1), 014010 (2007).
16. W. J. Cottrell, J. D. Wilson, and T. H. Foster, "Microscope enabling multimodality imaging, angle-resolved scattering, and scattering spectroscopy," *Opt. Lett.* **32**(16), 2348–2350 (2007).
17. D. W. Shipp, "Holographic angular domain elastic scattering of single biological cells," PhD Dissertation, Institute of Optics, University of Rochester, Rochester, NY (2014).
18. J. R. Mourant et al., "Mechanisms of light scattering from biological cells relevant to noninvasive optical-tissue diagnostics," *Appl. Opt.* **37** (16), 3586–3593 (1998).
19. J. R. Mourant et al., "Light scattering from cells: the contribution of the nucleus and the efects of prolierative status," *J. Biomed. Opt.* **5**(2), 131–137 (2000).
20. J. D. Wilson and T. H. Foster, "Mie theory interpretations of light scattering from intact cells," *Opt. Lett.* **30**(18), 2442–2444 (2005).
21. B. Harding, C. Tremblay, and D. Cousineau, "Standard errors: a review and evaluation of standard error estimators using Monte Carlo simulations," *Quant. Methods Psychol.* **10**(2), 107–123 (2014).
22. Z. J. Smith and A. J. Berger, "Validation of an integrated Raman- and angular-scattering microscopy system on heterogeneous bead mixtures and single human immune cells," *Appl. Opt.* **48**(10), D109–D120 (2009).
23. J. W. Pyhtila, R. N. Graf, and A. Wax, "Determining nuclear morphology using an improved angle-resolved low coherence interferometry system," *Opt. Express* **11** (25), 3473–3484 (2003).
24. J. Zheng and N. N. Boustany, "Alterations in the characteristic size distributions of subcellular scatterers at the onset of apoptosis: effect of Bcl-xL and Bax/Bak," *J. Biomed. Opt.* **15**(4), 045002 (2010).

25. M. Kalashnikov et al., "Assessing light scattering of intracellular organelles in single intact living cells," *Opt. Express* **17**(22), 19674–19681 (2009).
26. H. Ding et al., "Fourier transform light scattering of inhomogeneous and dynamic structures," *Phys. Rev. Lett.* **101**(23), 238102 (2008).
27. W. Choi et al., "Field-based angle-resolved light-scattering study of single live cells," *Opt. Lett.* **33**(**14**), 1596–1598 (2008).

Biographies of the authors are not available.